MATERIALS CHEMISTRY FRONTIERS

CHINESE CHEMICAL SOCIETY

ROYAL SOCIETY OF CHEMISTRY

RESEARCH ARTICLE

View Article Online
View Journal | View Issue

Cite this: *Mater. Chem. Front.*, 2022, **6**, 924

New aggregation-induced delayed fluorescent materials for efficient OLEDs with high stabilities of emission color and efficiency†

Hao Chen,[a] Huijun Liu,[a] Yi Xiong,[a] Junchu He,[a] Zujin Zhao *[a] and Ben Zhong Tang [abc]

Received 16th December 2021,
Accepted 10th February 2022

DOI: 10.1039/d1qm01625c

rsc.li/frontiers-materials

Thermally activated delayed fluorescence (TADF) can harvest both singlet and triplet excitons to achieve high electroluminescence (EL) efficiency for organic light-emitting diodes (OLEDs). However, many TADF emitters generally suffer from severe emission quenching and exciton annihilation at high voltages or luminance. To address this issue, in this work, two new luminogens, CDBP-BP-PXZ and CDBP-BP-DMAC, consisting of an electron-withdrawing benzoyl group and electron-donating 9,9′-(2,2′-dimethyl-[1,1′-biphenyl]-4,4′-diyl)bis(9*H*-carbazole) and phenoxazine/9,9-dimethyl-9,10-dihydroacridine are synthesized and characterized. They exhibit high thermal and electrochemical stabilities and show interesting aggregation-induced delayed fluorescence properties. They exhibit good EL performances in nondoped and doped OLEDs with high electroluminescence (EL) efficiencies, very small efficiency roll-offs and high emission color stability. The excellent EL performance of both luminogens disclose their good application potential in practical display and lighting devices.

Introduction

In the past decades, organic light-emitting diodes (OLEDs) have achieved great progress in full-color displays and solid-state lighting sources, owing to their practical advantages, such as self-luminescence, low cost, flexibility, high efficiency, energy conservation, and so forth.[1–5] In the rapid development of OLEDs, the exploration of efficient and stable luminescent materials plays the most important role. Conventional fluorescent materials can only harness electrogenerated 25% singlet excitons, which limits the enhancement of their electroluminescence (EL) efficiencies.[6–9] To date, there are some methods for enhancing exciton utilization, such as phosphorescence,[10–12] triplet–triplet annihilation (TTA),[13–16] singlet fission (SF),[17] hybridized local and charge-transfer (HLCT)[18–20] and thermally activated delayed fluorescence (TADF).[21–25]

Among them, purely organic TADF materials have received significant attention as the core materials for the third generation OLEDs owing to their high internal quantum efficiencies (IQEs) of 100% achieved through thermally activated reverse intersystem crossing (RISC) based on small energy gaps (ΔE_{ST}s) between the lowest singlet excited state (S_1) and the lowest triplet excited state (T_1).[26–30] Therefore, OLEDs based on low cost TADF materials can realize high electroluminescence (EL) efficiencies, comparable to those based on noble metal-containing phosphorescence materials.[31–36] However, many TADF materials suffer from serious concentration quenching and exciton annihilation because of the long lifetimes of the triplet excited states.[37–40] Although this situation can be addressed to some extent by employing a blend film containing the host and the dopant as an emitting layer (EML) to reduce concentration quenching, the doped devices still encounter drastic efficiency roll-offs at high voltages, which becomes a troublesome obstacle for the commercial application of TADF materials.[41–45]

Aggregation-induced delayed fluorescence (AIDF) emitters, which exhibit both TADF and aggregation-induced emission (AIE) properties, are emerging as promising alternatives to overcome these drawbacks.[46–50] Actually, OLEDs based on AIDF

[a] *State Key Laboratory of Luminescent Materials and Devices, Guangdong Provincial Key Laboratory of Luminescence from Molecular Aggregates, South China University of Technology, Guangzhou 510640, China. E-mail: mszjzhao@scut.edu.cn*

[b] *Shenzhen Institute of Aggregate Science and Technology, School of Science and Engineering, The Chinese University of Hong Kong, Shenzhen, Guangdong 518172, China*

[c] *AIE Institute, Guangzhou Development District, Huangpu, Guangzhou 510530, China*

† Electronic supplementary information (ESI) available: Materials and instruments, photophysical data, PL spectra and transient PL decay curves in the THF/water mixture, PL spectra in different solvents, temperature-dependent transient PL decay curves, PL decay curves in THF solutions under air and N_2 atmospheres, fluorescence and phosphorescence spectra at 77 K, carrier mobility spectra and EL performance data in doped devices with different hosts. See DOI: 10.1039/d1qm01625c

luminogens have presented excellent EL performances in nondoped and doped devices, comparable to conventional TADF materials but with noticeably enhanced efficiency stability.[51–58] So, in this work, we wish to report two novel AIDF luminogens CDBP-BP-PXZ and CDBP-BP-DMAC, constructed using electron-donors of 9,9′-(2,2′-dimethyl-[1,1′-biphenyl]-4,4′-diyl) bis(9*H*-carbazole) (CDBP) and phenoxazine (PXZ)/9,9-dimethyl-9,10-dihydroacridine (DMAC) and an electron-acceptor of the benzoyl group. The carbonyl therein can achieve effective n–π* transition, which is important to enlarge the spin–orbit coupling (SOC) to facilitate intersystem crossing (ISC) and RISC processes. By comprehensive investigation, both luminogens exhibit high emission efficiencies and prominent delayed fluorescence in the solid state, which make them ideal emitters for OLEDs. The nondoped and doped OLEDs adopting both luminogens as emissive layers display excellent EL efficiencies with very small efficiency roll-offs and high emission color stabilities.

Results and discussion

Synthesis and characterization

The new luminogens CDBP-BP-PXZ and CDBP-BP-DMAC are prepared through two-step reactions according to the synthetic routes illustrated in Scheme 1. The Friedel–Crafts acylation reaction of CDBP with 4-fluorobenzoyl chloride yields an important intermediate CDBP-BP-F, followed by coupling with PXZ and DMAC to afford target molecules CDBP-BP-PXZ and CDBP-BP-DMAC, respectively, in good yields. Both molecular structures are well characterized using NMR and high-resolution mass spectra (HRMS). The detailed synthetic procedures and characterization data of CDBP-BP-PXZ and CDBP-BP-DMAC are presented in the Experimental section. They have good solubility in common organic solvents such as dichloromethane, chloroform, tetrahydrofuran (THF), and so forth, but are hardly soluble in water.

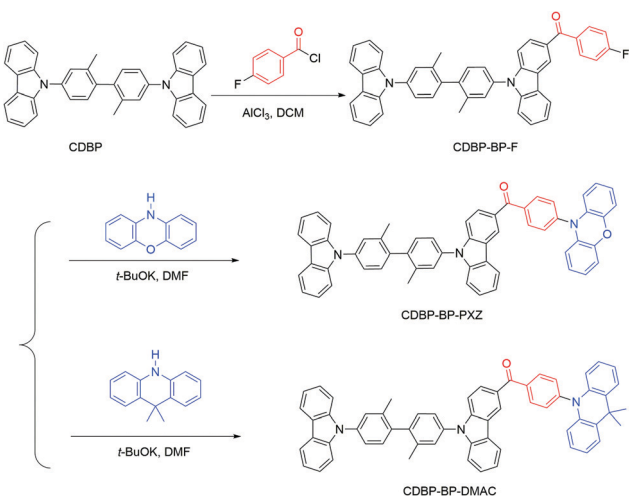

Scheme 1 Synthetic routes and chemical structures of CDBP-BP-PXZ and CDBP-BP-PXZ.

The thermal stability of both luminogens is evaluated through thermogravimetric analysis (TGA) at a heating rate of 10 °C min^{-1} under a nitrogen atmosphere. As illustrated in Fig. 1A, both luminogens exhibit high thermal stabilities, with very high decomposition temperatures (T_d, corresponding to 5% weight loss) of 454 °C and 450 °C for CDBP-BP-PXZ and CDBP-BP-DMAC, respectively. These high T_ds are beneficial for the fabrication of OLEDs using a vacuum deposition process. The glass-transition temperatures of both luminogens are not detected.

Electrochemical properties

Cyclic voltammetry (CV) is carried out on the CDBP-BP-PXZ and CDBP-BP-DMAC solutions to determine the practical HOMO and LUMO energy levels. As illustrated in Fig. 1B, both luminogens show similar voltammograms with close oxidation and reduction peaks. The oxidation potential and reduction potentials are 0.26 and −2.03 V against the Fc/Fc^+ redox couple, corresponding to a HOMO energy level of −5.06 eV and a LUMO energy level of −2.77 eV for CDBP-BP-PXZ, and the oxidation potential and reduction potentials are 0.47 and −2.13 V against the Fc/Fc^+ redox couple, corresponding to a HOMO energy level of −5.27 eV and a LUMO energy level of −2.67 eV for CDBP-BP-DMAC (HOMO = $-[E_{ox} + 4.8]$ eV; LUMO = $-[E_{re} + 4.8]$ eV, where E_{ox} and E_{re} represent the onset potentials of oxidation and reduction relative to Fc/Fc^+, respectively).

Electronic structures

The geometrical and electronic structures of CDBP-BP-PXZ and CDBP-BP-DMAC are investigated *via* a theoretical simulation conducted *via* density functional theory (DFT) and time-dependent density functional theory (TD-DFT) calculations with the PBE0/6-31G(d,p) basis set. The optimized molecular conformations and calculated frontier orbital distributions of CDBP-BP-PXZ and CDBP-BP-DMAC are displayed in Fig. 2. Both luminogens have highly twisted structures with a separated distribution of the frontier orbitals. The LUMOs are mainly localized on the electron-accepting carbonyl group and parts of

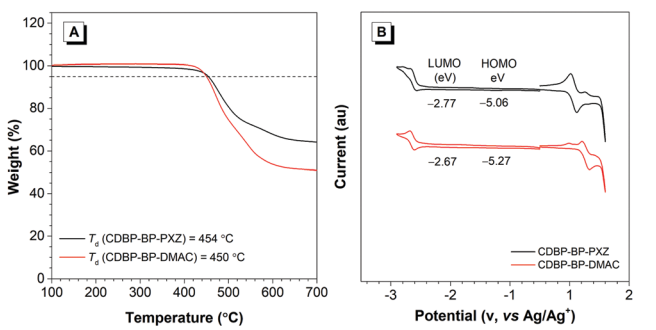

Fig. 1 (A) TGA thermograms of CDBP-BP-PXZ and CDBP-BP-DMAC, recorded under a nitrogen atmosphere at a heating rate of 10 °C min^{-1}; (B) cyclic voltammograms of the solutions of CDBP-BP-PXZ and CDBP-BP-DMAC, measured in dichloromethane (HOMO) and dimethylformamide (LUMO) containing 0.1 M tetrabutylammonium hexafluorophosphate. Scan rate: 100 mV s^{-1}.

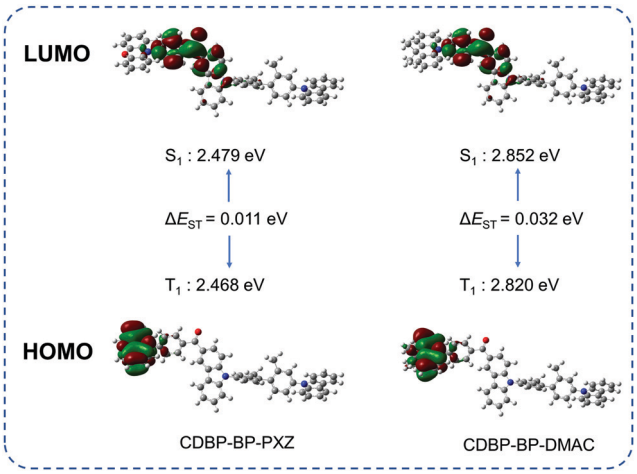

Fig. 2 Spatial distributions of HOMOs and LUMOs, and ΔE_{ST} values of the two luminogens, calculated using the PBE0 hybrid functional at the basis set level of 6-31G(d,p).

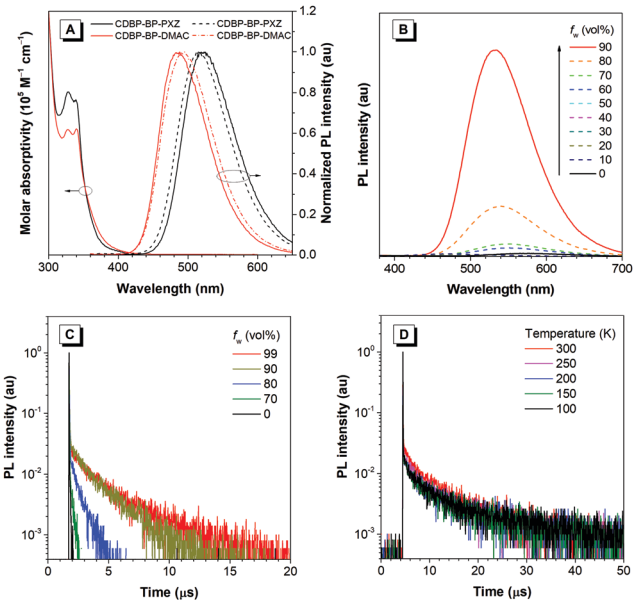

Fig. 3 (A) Absorption spectra of CDBP-BP-PXZ and CDBP-BP-DMAC in THF solutions (10^{-5} mol L^{-1}) and their normalized PL spectra in neat films (solid line) and doped films (dashed line); (B) PL spectra of CDBP-BP-PXZ and (C) transient PL decay curves of CDBP-BP-DMAC in THF/water mixtures with different water fractions (f_w), where the concentration of CDBP-BP-PXZ and CDBP-BP-DMAC is 10^{-5} mol L^{-1}; (D) temperature-dependent transient PL decay spectra of CDBP-BP-DMAC in neat films, recorded under a nitrogen atmosphere.

adjacent aromatic rings, while the HOMOs are predominantly focused on the electro-donating PXZ and DMAC units. However, CDBP shows no contribution to the HOMOs of both molecules. Hence, the HOMO and the LUMO are almost completely separated, due to the nearly perpendicular connection of BP and PXZ/DMAC. The efficient separation of HOMOs and LUMOs endows CDBP-BP-PXZ and CDBP-BP-DMAC with small theoretical ΔE_{ST} values of 0.011 and 0.032 eV, respectively, which are small enough to allow an efficient RISC process from T_1 to S_1 states.

Photophysical properties

CDBP-BP-PXZ and CDBP-BP-DMAC show analogous absorption spectra in oxygen-free THF solutions with strong absorption bands at around 327 nm and 328 nm (Fig. 3A), respectively, which are generated due to the π–π* transition. Moreover, weak and broad absorption bands extending to 430 nm are also observed, which can be attributed to the twisted intramolecular charge transfer (TICT) state between the benzoyl core and the PXZ and DMAC moieties. The photoluminescence (PL) properties are also measured in solutions and films. In THF solutions, CDBP-BP-PXZ and CDBP-BP-DMAC emit weakly at 575 and 534 nm, with low PL quantum yields (Φ_{PL}s) of 2.6% and 10.9%, respectively. Because the electron-donating capacity of the DMAC group is weaker than that of the PXZ group, CDBP-BP-DMAC shows weaker TICT effects and thus bluer and stronger emission than CDBP-BP-PXZ. However, the vacuum-deposited neat films of CDBP-BP-PXZ and CDBP-BP-DMAC radiate strong green and sky-blue lights with PL peaks at 528 nm and 488 nm, respectively. The blue-shifted emissions from THF solutions to neat films are attributed to the decreased polarity of the environment, in which the luminogenic molecules experience a weakened ICT effect. Meanwhile, the Φ_{PL}s are greatly enhanced to 77.4% and 59.2%, respectively, in neat films, being more than 28 times for CDBP-BP-PXZ and 5 times for CDBP-BP-DMAC in THF solutions, demonstrating that both luminogens have noticeable AIE properties.[59,60]

To further investigate the PL properties of both luminogens, the PL spectra in THF/water binary solutions with varied water fractions (f_w) from 0% to 90% are recorded, where the THF solution is a good solvent but water is poor for both luminogens (Fig. 3B and Fig. S1, ESI†). By adding a small volume of water into the THF solutions, the PL intensities are slightly decreased, which is due to the enhanced TICT effect because of the increased polarity of the mixture.[61,62] The TICT effect can be verified through a solvatochromism experiment, in which the PL peak is red-shifted obviously along with the increase of solvent polarity (Fig. S2, ESI†). But the aggregates are formed when a large volume of water is added into the THF solutions, and the PL intensities are greatly enhanced and apparently blue-shifted, which can be attributed to the restriction of intramolecular motion and thus the suppression of the non-radiative decay. Moreover, both luminogens show very short PL lifetimes in THF solutions. However, by adding a large amount of water to the THF solutions, the PL lifetimes are greatly increased and the delayed fluorescence proportions exhibit a prominently growing trend (Fig. 3C and Fig S3, ESI†). Combining the excellent PL properties of both luminogens in neat films, it is clear that CDBP-BP-PXZ and CDBP-BP-DMAC show typical AIE characteristics.

In THF solutions, both luminogens show weak emission and faint delayed fluorescence, with short PL lifetimes of 34.9 and 14.0 ns of CDBP-BP-PXZ and CDBP-BP-DMAC, respectively, due to the vigorous intramolecular motions, which can non-radiatively deactivate the excited state and undermine the ISC and RISC

Table 1 The photophysical data of CDBP-BP-PXZ and CDBP-BP-DMAC

		λ_{abs} (nm)	λ_{em} (nm)	Φ_{PL}[c] (%)	$\langle\tau\rangle$[d] (ns)	τ_{prompt}[e] (ns)	$\tau_{delayed}$[e] (μs)	$R_{delayed}$[f] (%)	ΔE_{ST}[g] (eV)	k_{RISC}[h] ($\times 10^5$ s^{-1})
CDBP-BP-PXZ	Solution[a]	327	575	2.6	34.9	—	—	—	—	—
	Neat film[b]	344	523	77.4	509.4	26.0	2.5	19.5	0.039	4.97
	Doped film[b]	332	515	93.2	293.9	27.0	2.7	10%	0.096	4.12
CDBP-BP-DMAC	Solution[a]	328	534	10.9	14.0	—	—	—	—	—
	Neat film[b]	345	488	59.2	2009.3	19.1	6.1	32.4	0.043	2.43
	Doped film[b]	344	495	71.4	2432.9	22.1	6.1	39.4	0.043	2.71

[a] Measured in THF solution (10^{-5} M) at room temperature. [b] Neat film and doped film (for CDBP-BP-PXZ: 20 wt% doping concentration with CBP as the host; for CDBP-BP-DMAC: 40 wt% doping concentration with PPF as the host), vacuum-deposited on a quartz substrate. [c] Determined using a calibrated integrating sphere under nitrogen at room temperature. [d] Mean fluorescence lifetime evaluated at 300 K under nitrogen. [e] Fluorescence lifetimes of prompt (τ_{prompt}) and delayed ($\tau_{delayed}$) components evaluated at 300 K under nitrogen. [f] Ratio of the delayed component. [g] ΔE_{ST} = singlet–triplet energy splitting. [h] Rate constant of the reverse intersystem crossing process.

processes. But from the PL decay curves in THF solutions under air and N_2 atmospheres (Fig. S4, ESI†), it can be found that the PL lifetime is obviously increased in the absence of O_2 for CDBP-BP-DMAC, implying the involvement of the triplet state. In neat films, CDBP-BP-PXZ and CDBP-BP-DMAC exhibit distinct delayed fluorescence with lifetimes of 509.4 and 2009.3 ns and ratios of 19.5% and 32.4%, respectively. The RISC rate constants (k_{RISC}) are 4.97 $\times$ 10^5 s^{-1} and 2.43 $\times$ 10^5 s^{-1} for CDBP-BP-PXZ and CDBP-BP-DMAC, respectively (Table 1). Moreover, it can be found from the temperature-dependent transient PL decay spectra (Fig. 3D and Fig. S5, ESI†) that the PL lifetime is increased prominently as the temperature increases from 100 to 300 K, demonstrating that the delayed fluorescence properties originate from triplet to singlet conversion *via* the RISC process under thermal activation. A small ΔE_{ST} is favorable for an efficient RISC process to achieve the occurrence of delayed fluorescence. According to the fluorescence and phosphorescence spectra of the neat films recorded at 77 K (Fig. S6, ESI†), the values of ΔE_{ST} are acquired from the onsets of the spectra and measured to be 0.039 eV for CDBP-BP-PXZ and 0.043 eV for CDBP-BP-DMAC, which are small enough to ensure the RISC process and thus the generation of delayed fluorescence. The above results indicate that CDBP-BP-PXZ and CDBP-BP-DMAC possess evident AIDF features.

To further decipher their PL behaviours, the doped films of CDBP-BP-PXZ and CDBP-BP-DMAC (20 wt% CDBP-BP-PXZ in the 4,4′-di(9*H*-carbazol-9-yl)-1,1′-biphenyl (CBP) host and 40 wt% CDBP-BP-DMAC in the bis-(diphenylphosphoryl)-dibenzo[b,d]-furan (PPF) host) are prepared and studied. The doped film of CDBP-BP-PXZ emits strong green fluorescence with a peak at 515 nm and a high Φ_{PL} of 93.2%. The doped film of CDBP-BP-DMAC exhibits sky-blue fluorescence with a peak at 495 nm and a Φ_{PL} of 71.4%. The PL lifetime of CDBP-BP-PXZ in doped films is as short as 293.9 ns and the ratio of the delayed component is 10.0%. And the value of ΔE_{ST} is 0.096 eV, which is small enough for an efficient RISC process. As for CDBP-BP-DMAC in the doped film, the PL lifetime and the ratio of delayed component are increased slightly and the value of ΔE_{ST} is 0.043 eV, close to that in the neat film.

Electroluminescence

In view of the efficient PL performance with prominently delayed fluorescence in films, the EL performances of CDBP-BP-PXZ and CDBP-BP-DMAC in OLEDs are investigated. Nondoped OLEDs with a configuration of ITO/HATCN (5 nm)/TAPC (25 nm)/TCTA (5 nm)/emitter (35 nm)/TmPyPB (55 nm)/LiF (1 nm)/Al (120 nm) (device I: emitter = CDBP-BP-PXZ; device II: emitter = CDBP-BP-DMAC) are fabricated using a vacuum-deposition technique, in which the neat films of CDBP-BP-PXZ and CDBP-BP-DMAC function as emitters, hexaazatriphenylenehexacabonitrile (HATCN) serves as the hole-injection layer, 1,1′-bis(di-4-tolylaminophenyl) cyclohexane (TAPC) and 1,3,5-tri(*m*-pyrid-3-yl-phenyl)benzene (TmPyPB) work as the hole- and electron-transporting layers, respectively, and tris[4-(carbazol-9-yl)phenyl]amine (TCTA) functions as the electron-blocking layer (Fig. 4). Both devices are turned on at low voltages of 2.6 V and 2.8 V, indicating that holes and electrons can be effectively injected and transported into emitting layers for exciton generation. Device I of CDBP-BP-PXZ exhibits strong green light with an EL peak at 536 nm and shows a maximum luminance (L_{max}) of up to 53 539 cd m^{-2} (Table 2). The maximum current efficiency (η_C), power efficiency (η_P) and external quantum efficiency (η_{ext}) of device I are 50.5 cd A^{-1}, 46.5 lm W^{-1} and 15.5%, respectively. More importantly, even at 1000 cd m^{-2}, device I still holds η_C, η_P and η_{ext} of 50.3 cd A^{-1}, 39.5 lm W^{-1} and 15.4%, respectively, revealing that device I has excellent efficiency stability. Device II of CDBP-BP-DMAC exhibits strong sky-blue light at a peak of 496 nm and shows an L_{max} of up to 13 505 cd m^{-2}. The maximum η_C, η_P and η_{ext} values of device III are 24.4 cd A^{-1}, 22.2 lm W^{-1} and 9.5%, respectively. The η_{ext} of this device remains at 9.3% at 1000 cd m^{-2}, exhibiting a negligible efficiency roll-off (Fig. 5A–D). In addition, both nondoped devices exhibit high stabilities of emission color, and the emission spectra show a negligible offset with the increase of voltage from

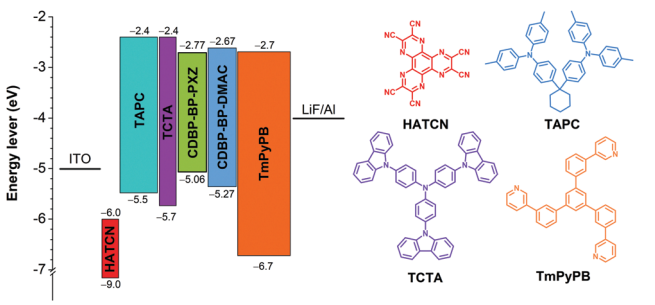

Fig. 4 Energy level diagrams of non-doped OLEDs based on CDBP-BP-PXZ and CDBP-BP-DMAC.

Table 2 The performance data of the OLEDs based on CDBP-BP-PXZ and CDBP-BP-DMAC

Device[a]	V_{on} (V)	L_{max} (cd m^{-2})	η_C (cd A^{-1})	η_P (lm W^{-1})	η_{ext} (%)	CIE (x, y)	λ_{EL} (nm)
			Maximum value/at 1000 cd m^{-2}				
I	2.6	53 539	50.5/50.3	46.5/39.5	15.5/15.4	(0.355, 0.579)	536
II	2.8	13 505	24.4/23.9	22.2/18.8	9.5/9.3	(0.229, 0.445)	496
III	3.0	60 899	67.1/65.4	56.5/46.7	20.8/20.3	(0.322, 0.575)	528
IV	2.8	31 007	44.9/41.0	50.4/29.3	16.8/15.4	(0.227, 0.466)	504

[a] Abbreviation: V_{on} = turn-on voltage at 1 cd m^{-2}; L_{max} = maximum luminance; η_C = current efficiency; η_P = power efficiency; η_{ext} = external quantum efficiency; CIE = Commission Internationale de l'Eclairage coordinates at 1000 cd m^{-2}; λ_{EL} = electroluminescence peak at 1000 cd m^{-2}.

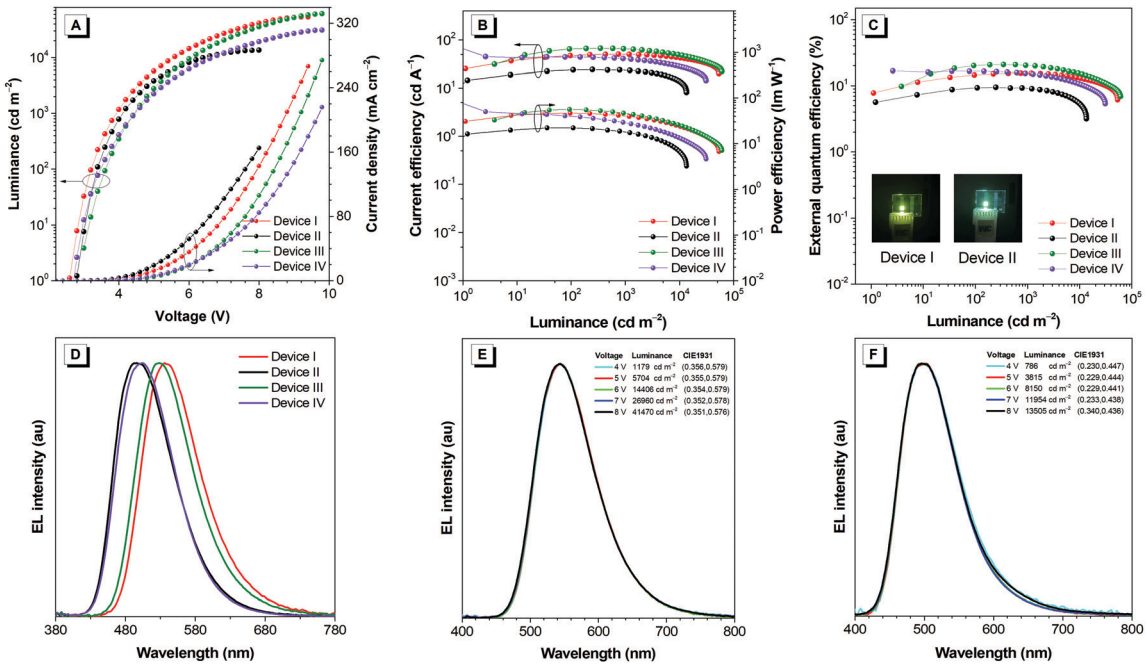

Fig. 5 (A) Luminance and current density curves with the change of voltage of devices I–IV; (B) current efficiency and power efficiency curves with the change of luminance of devices I–IV; (C) external quantum efficiency curves with the change of luminance. Inset: The photo of devices I and II at 10 mA cm^{-2}; (D) EL spectra at 10 mA cm^{-2} of devices I–IV; (E) and (F) EL spectra of the CDBP-BP-PXZ in device I and CDBP-BP-DMAC in device II at varied luminance.

4 to 8 V (Fig. 5E and F), which is attributed to the balanced carrier transport of the devices and stable recombination region of the excitons. The space charge limited current (SCLC) method was also carried out to evaluate the carrier transport ability of both luminogens with the structures of ITO/TAPC (10 nm)/luminogens (80 nm)/TAPC (10 nm)/Al (hole-only device) and ITO/TmPyPB (10 nm)/luminogens (80 nm)/TmPyPB (10 nm)/LiF (1 nm)/Al (electron-only device), respectively.[63] As shown in Fig. S7 (ESI†), at an electric field of 5.5×10^5 V cm^{-1}, the electron mobilities of CDBP-BP-PXZ and CDBP-BP-DMAC are determined to be 1.36×10^{-7} and 1.35×10^{-5} cm^2 V^{-1} s^{-1}, while the hole mobilities are 1.57×10^{-5} and 1.92×10^{-5} cm^2 V^{-1} s^{-1}, respectively. It can be found that CDBP-BP-DMAC shows better bipolar carrier transport ability than CDBP-BP-PXZ.

To further evaluate the potential application of both luminogens, doped OLEDs with a configuration of ITO/HATCN (5 nm)/TAPC (25 nm)/TCTA (5 nm)/CBP: 20 wt% CDBP-BP-DMAC (35 nm)/TmPyPB (55 nm)/LiF (1 nm)/Al (120 nm) for device III and ITO/HATCN (5 nm)/TAPC (25 nm)/TCTA (5 nm)/PPF: 40 wt% CDBP-BP-DMAC (35 nm)/PPF (10 nm)/TmPyPB (55 nm)/LiF (1 nm)/Al (120 nm) for device IV are fabricated, where the CBP acts as a host and PPF serves as a host and a hole-blocking layer. Both doped OLEDs of CDBP-BP-PXZ and CDBP-BP-DMAC show low turn-on voltages at 3.0 V and 2.8 V, EL peaks of 528 nm and 504 nm, and high luminance of 60 899 cd m^{-2} and 31 007 cd m^{-2}. The doped OLED of CDBP-BP-PXZ shows higher peaks and η_C, η_P and η_{ext} of 67.1 cd A^{-1}, 56.5 lm W^{-1} and 20.8%, respectively. The doped OLED of CDBP-BP-DMAC also achieves high maximum values for η_C, η_P and η_{ext} of 44.9 cd A^{-1}, 50.4 lm W^{-1} and 16.8%, respectively. Both doped OLEDs hold a very small efficiency roll-off at 1000 cd m^{-2} with high η_{ext} values of 20.3% and 15.4%. All these results demonstrate that both nondoped and doped devices not only possess outstanding EL efficiencies but also exhibit superb efficiency stability. The improved EL performances in doped OLEDs relative to those in nondoped OLEDs can be attributed to the enhanced Φ_{PL} values. In addition, the

host materials also significantly influence the EL performances of both luminogens (Table S1, ESI), partially due to the host-tuning effect.[64]

Conclusions

In summary, two new luminogens CDBP-BP-PXZ and CDBP-BP-DMAC comprising an electron-withdrawing benzoyl group and electron-donating CDBP and PXZ/DMAC moieties are designed, synthesized and systematically investigated. Both luminogens have highly twisted structures to achieve small ΔE_{ST} values. They exhibit high thermal and electrochemical stabilities and typical AIDF characteristics. The non-doped and doped devices using CDBP-BP-PXZ as the emitter radiates strongly with high EL efficiencies of up to 15.5%, and 20.8%, respectively. By adopting CDBP-BP-DMAC as the emitter, sky-blue emissions with high EL efficiencies of 9.5% and 16.8% are achieved in non-doped and doped devices, respectively. More importantly, both non-doped and doped devices show excellent emission color stability and very small efficiency roll-offs at 1000 cd m^{-2}. These excellent EL performances of CDBP-BP-PXZ and CDBP-BP-DMAC demonstrate their great application potential in OLEDs.

Experimental section

Synthesis and characterization

9-(4′-(9*H*-Carbazol-9-yl)-2,2′-dimethyl-[1,1′-biphenyl]-4-yl)-(9*H*-carbazol-3-yl)(4-fluorophenyl)methanone (CDBP-BP-F). Aluminum trichloride (0.467 g, 3.50 mmol) was added to a stirred solution of 9,9′-(2,2′-dimethyl-[1,1′-biphenyl]-4,4′-diyl)bis(9*H*-carbazole) (1.874 g, 3.3 mmol) and 4-fluorobenzoyl chloride (0.632 g, 4 mmol) in dehydrated dichloromethane (50 mL) in an ice bath for 15 min. Then, the reaction mixture was warmed to room temperature and stirred for 3 h. The reaction was quenched with ice water and hydrochloric acid (30 mL, 2 : 1 v/v), and extracted with dichloromethane several times. The combined organic layers were washed twice with water, and then dried over anhydrous $MgSO_4$. After filtration and solvent evaporation under reduced pressure, the residue was purified by column chromatography on silica gel (dichloromethane: petroleum ether, 1 : 2 v/v) to afford CDBP-BP-F as a white solid in 57.4% yield (1.422 g). ^{1}H NMR (400 MHz, CD_2Cl_2) δ 8.65 (s, 1H), 8.35–8.05 (m, 3H), 8.02–7.78 (m, 3H), 7.68–7.10 (m, 18H), 2.44–2.13 (m, 6H). ^{13}C NMR (10 MHz, CD_2Cl_2) δ 194.68, 166.25, 163.75, 143.46, 141.88, 140.93, 140.83, 139.89, 138.44, 138.07, 136.89, 136.02, 135.20, 135.17, 132.46, 132.37, 131.05, 130.78, 129.46, 128.35, 128.29, 126.78, 125.93, 124.23, 123.58, 123.36, 123.32, 122.98, 120.87, 120.59, 120.24, 119.90, 115.35, 115.14, 110.46, 109.88, 109.65, 19.90, 19.87. HRMS ($C_{45}H_{31}FN_2O$): *m*/*z* 634.2420 [M^+, calcd 634.2415].

(4-(10*H*-Phenoxazin-10-yl)phenyl)(9-(4′-(9*H*-carbazol-9-yl)-2,2′-dimethyl-[1,1′-biphenyl]-4-yl)-9H-carbazol-3-yl)methanone (CDBP-BP-PXZ). A mixture of CDBP-BP-F (0.90 g, 1.2 mmol) and 10*H*-phenoxazine (0.26 g, 1.4 mmol) in deaerated and dehydrated *N*,*N*-dimethylformamide (20 mL) was stirred for 15 min under nitrogen at room temperature, and then potassium *tert*-butoxide (0.27 g, 2.4 mmol) was added, followed by stirring at 120 °C for 12 h. The reaction was quenched with water (20 mL) and extracted with dichloromethane several times. The combined organic layers were washed twice with water, and then dried over anhydrous $MgSO_4$. After filtration and solvent evaporation under reduced pressure, the residue was purified by column chromatography on silica gel (dichloromethane : petroleum ether, 1 : 1 v/v) to afford a yellow solid of CDBP-BP-PXZ in 72.1% yield (0.69 g). ^{1}H NMR (400 MHz, $CDCl_3$) δ 8.78 (d, J = 1.6 Hz, 1H), 8.25 (d, J = 8.0 Hz, 1H), 8.18 (d, J = 7.6 Hz, 2H), 8.14–8.07 (m, 2H), 8.07–8.03 (m, 1H), 7.62–7.37 (m, 16H), 7.35–7.29 (m, 2H), 6.76–6.63 (m, 6H), 6.09–6.00 (m, 2H), 2.40–2.25 (m, 6H). ^{13}C NMR (100 MHz, $CDCl_3$) δ 195.50, 191.21, 159.57, 144.04, 143.68, 142.41, 141.90, 140.92, 140.86, 139.70, 138.84, 138.36, 137.86, 137.08, 136.07, 133.92, 132.72, 131.07, 130.76, 129.13, 128.77, 128.42, 128.39, 126.94, 125.95, 124.40, 124.37, 123.83, 123.44, 123.34, 123.27, 121.79, 121.08, 120.82, 120.39, 119.98, 115.71, 113.42, 110.54, 109.91, 109.72, 20.22, 20.18. HRMS ($C_{57}H_{39}N_3O_2$): *m*/*z* 797.3037 [M^+, calcd 797.3042].

(9-(4′-(9*H*-Carbazol-9-yl)-2,2′-dimethyl-[1,1′-biphenyl]-4-yl)-9*H*-carbazol-3-yl)(4-(9,9-dimethylacridin-10(9H)-yl)phenyl)methanone (CDBP-BP-DMAC). The procedures are analogous to those described for CDBP-BP-PXZ. Yellow-green solid; yield 67.5%. ^{1}H NMR (400 MHz, $CDCl_3$) δ 8.81 (d, J = 1.7 Hz, 1H), 8.26 (d, J = 7.7 Hz, 1H), 8.20–8.13 (m, 4H), 8.11–8.07 (m, 1H), 7.63–7.29 (m, 21H), 7.09–6.92 (m, 4H), 6.47–6.34 (m, 2H), 2.31 (d, J = 7.6 Hz, 6H), 1.72 (s, 6H). ^{13}C NMR (100 MHz, $CDCl_3$) δ 195.70, 144.75, 143.66, 141.90, 140.93, 140.84, 140.61, 139.72, 138.49, 138.35, 137.87, 137.07, 136.10, 132.61, 131.06, 130.74, 130.49, 129.28, 128.82, 128.42, 128.40, 126.91, 126.46, 125.95, 125.37, 124.38, 123.86, 123.46, 123.44, 123.27, 121.07, 121.02, 120.82, 120.39, 119.98, 114.31, 110.52, 109.91, 109.71, 36.10, 31.18, 20.22, 20.19. HRMS ($C_{60}H_{45}N_3O$): *m*/*z* 823.3564 [M^+, calcd 823.3563].

Conflicts of interest

There is no conflict to declare.

Acknowledgements

This study was financially supported by the National Natural Science Foundation of China (21788102 and 51620105009), the Natural Science Foundation of Guangdong Province (2019B030301003) and the Fundamental Research Funds for the Central Universities.

Notes and references

1 C. W. Tang and S. A. VanSlyke, Organic electroluminescent diodes, *Appl. Phys. Lett.*, 1987, **51**, 913–915.

2 H. Sasabe and J. Kido, Development of high performance OLEDs for general lighting, *J. Mater. Chem. C*, 2013, **1**, 1699–1707.
3 C. Adachi and A. S. D. Sandanayaka, The leap from organic light-emitting diodes to organic semiconductor laser diodes, *CCS Chem.*, 2020, **2**, 1203–1216.
4 A. Salehi, X. Fu, D. H. Shin and F. So, Recent advances in OLED optical design, *Adv. Funct. Mater.*, 2019, **29**, 1088803.
5 J. Yang, L. Li, Y. Yu, Z. Ren, Q. Peng, S. Ye, Q. Li and Z. Li, Blue pyrene-based AIEgens: Inhibited intermolecular π–π stacking through the introduction of substituents with controllable intramolecular conjugation, and high external quantum efficiencies up to 3.46% in non-doped OLEDs, *Mater. Chem. Front.*, 2017, **1**, 91–99.
6 D. Y. Kondakov, Role of triplet–triplet annihilation in highly efficient fluorescent devices, *J. Soc. Inf. Disp.*, 2009, **17**, 137.
7 B. Wex and B. R. Kaafarani, Perspective on carbazole-based organic compounds as emitters and hosts in TADF applications, *J. Mater. Chem. C*, 2017, **5**, 8622–8653.
8 Z. Xu, B. Z. Tang, Y. Wang and D. Ma, Recent advances in high performance blue organic light-emitting diodes based on fluorescence emitters, *J. Mater. Chem. C*, 2020, **8**, 2614–2642.
9 D. Y. Kondakov, Characterization of triplet–triplet annihilation in organic light-emitting diodes based on anthracene derivatives, *J. Appl. Phys.*, 2007, **102**, 114504.
10 K. Udagawa, H. Sasabe, C. Cai and J. Kido, Low-driving-voltage blue phosphorescent organic light-emitting devices with external quantum efficiency of 30%, *Adv. Mater.*, 2014, **26**, 5062–5066.
11 H. H. Kuo, Z. L. Zhu, C. S. Lee, Y. K. Chen, S. H. Liu, P. T. Chou, A. K. Jen and Y. Chi, Bis-tridentate iridium(III) phosphors with very high photostability and fabrication of blue-emitting OLEDs, *Adv. Sci.*, 2018, **5**, 1800846.
12 T. Zhang, C. Shi, C. Zhao, Z. Wu, J. Chen, Z. Xie and D. Ma, Extremely low roll-off and high efficiency achieved by strategic exciton management in organic light-emitting diodes with simple ultrathin emitting layer structure, *ACS Appl. Mater. Interfaces*, 2018, **10**, 8148–8154.
13 D. Y. Kondakov, Characterization of triplet–triplet annihilation in organic light-emitting diodes based on anthracene derivatives, *J. Appl. Phys.*, 2007, **102**, 114504.
14 Z. Xu, B. Z. Tang, Y. Wang and D. Ma, Recent advances in high performance blue organic light-emitting diodes based on fluorescence emitters, *J. Mater. Chem. C*, 2020, **8**, 2614–2642.
15 D. Di, L. Yang, J. M. Richter, L. Meraldi, R. M. Altamimi, A. Y. Alyamani, D. Credgington, K. P. Musselman, J. L. MacManus-Driscoll and R. H. Friend, Efficient triplet exciton fusion in molecularly doped polymer light-emitting diodes, *Adv. Mater.*, 2017, **29**, 1605987.
16 Z. Wu, S. Song, X. Zhu, H. Chen, J. Chi, D. Ma, Z. Zhao and B. Z. Tang, Highly efficient deep-blue fluorescent OLEDs based on anthracene derivatives with a triplet–triplet annihilation mechanism, *Mater. Chem. Front.*, 2021, **5**, 6978–6986.
17 R. Nagata, H. Nakanotani, W. J. Potscavage, Jr. and C. Adachi, Exploiting singlet fission in organic light-emitting diodes, *Adv. Mater.*, 2018, **30**, 1801484.
18 H. Zhang, B. Zhang, Y. Zhang, Z. Xu, H. Wu, P.-A. Yin, Z. Wang, Z. Zhao, D. Ma and B. Z. Tang, A multifunctional blue-emitting material designed via tuning distribution of hybridized excited-state for high-performance blue and host-sensitized OLEDs, *Adv. Funct. Mater.*, 2020, **30**, 2002323.
19 W. Li, Y. Pan, R. Xiao, Q. Peng, S. Zhang, D. Ma, F. Li, F. Shen, Y. Wang, B. Yang and Y. Ma, Employing ~100% excitons in OLEDs by utilizing a fluorescent molecule with hybridized local and charge-transfer excited state, *Adv. Funct. Mater.*, 2014, **24**, 1609–1614.
20 H. Zhang, G. Li, X. Guo, K. Zhang, B. Zhang, X. Guo, Y. Li, J. Fan, Z. Wang, D. Ma and B. Z. Tang, High-performance ultraviolet organic light-emitting diode enabled by high-lying reverse intersystem crossing, *Angew. Chem., Int. Ed.*, 2021, **60**, 22241–22247.
21 K. Goushi, K. Yoshida, K. Sato and C. Adachi, Organic light-emitting diodes employing efficient reverse intersystem crossing for triplet-to-singlet state conversion, *Nat. Photon.*, 2012, **6**, 253–258.
22 S. Hirata, Y. Sakai, K. Masui, H. Tanaka, S. Y. Lee, H. Nomura, N. Nakamura, M. Yasumatsu, H. Nakanotani, Q. Zhang, K. Shizu, H. Miyazaki and C. Adachi, Highly efficient blue electroluminescence based on thermally activated delayed fluorescence, *Nat. Mater.*, 2015, **14**, 330–336.
23 Y. Yuan, Y. Hu, Y.-X. Zhang, J.-D. Lin, Y.-K. Wang, Z.-Q. Jiang, L.-S. Liao and S.-T. Lee, Over 10% EQE near-infrared electroluminescence based on a thermally activated delayed fluorescence emitter, *Adv. Funct. Mater.*, 2017, **27**, 1700986.
24 T. Yang, Z. Cheng, Z. Li, J. Liang, Y. Xu, C. Li and Y. Wang, Improving the efficiency of red thermally activated delayed fluorescence organic light-emitting diode by rational isomer engineering, *Adv. Funct. Mater.*, 2020, **30**, 2002681.
25 M. Godumala, S. Choi, M. J. Cho and D. H. Choi, Thermally activated delayed fluorescence blue dopants and hosts: from the design strategy to organic light-emitting diode applications, *J. Mater. Chem. C*, 2016, **4**, 11355–11381.
26 X. Cai, X. Li, G. Xie, Z. He, K. Gao, K. Liu, D. Chen, Y. Cao and S. J. Su, "Rate-limited effect" of reverse intersystem crossing process: The key for tuning thermally activated delayed fluorescence lifetime and efficiency roll-off of organic light emitting diodes, *Chem. Sci.*, 2016, **7**, 4264–4275.
27 P. Rajamalli, N. Senthilkumar, P. Gandeepan, P. Y. Huang, M. J. Huang, C. Z. Ren-Wu, C. Y. Yang, M. J. Chiu, L. K. Chu, H. W. Lin and C. H. Cheng, A new molecular design based on thermally activated delayed fluorescence for highly efficient organic light emitting diodes, *J. Am. Chem. Soc.*, 2016, **138**, 628–634.
28 D. Zhang, P. Wei, D. Zhang and L. Duan, Sterically shielded electron transporting material with nearly 100% internal quantum efficiency and long lifetime for thermally activated delayed fluorescent and phosphorescent OLEDs, *ACS Appl. Mater. Interfaces*, 2017, **9**, 19040–19047.

29 P. L. dos Santos, J. S. Ward, M. R. Bryce and A. P. Monkman, Using guest–host interactions to optimize the efficiency of TADF OLEDs, *J. Phys. Chem. Lett.*, 2016, **7**, 3341–3346.
30 C. Zhao, L. Chen, Y. Li, Y. Qiu and L. Duan, Understanding the operational lifetime expansion methods of thermally activated delayed fluorescence sensitized OLEDs: A combined study of charge trapping and exciton dynamics, *Mater. Chem. Front.*, 2019, **3**, 1181–1191.
31 A. Khan, X. Tang, C. Zhong, Q. Wang, S. Y. Yang, F. C. Kong, S. Yuan, A. S. D. Sandanayaka, C. Adachi, Z. Q. Jiang and L. S. Liao, Intramolecular-locked high efficiency ultrapure violet-blue (CIE-y <0.046) thermally activated delayed fluorescence emitters exhibiting amplified spontaneous emission, *Adv. Funct. Mater.*, 2021, **31**, 2009488.
32 W. Li, M. Li, W. Li, Z. Xu, L. Gan, K. Liu, N. Zheng, C. Ning, D. Chen, Y. C. Wu and S. J. Su, Spiral donor design strategy for blue thermally activated delayed fluorescence emitters, *ACS Appl. Mater. Interfaces*, 2021, **13**, 5302–5311.
33 Y. Chen, D. Zhang, Y. Zhang, X. Zeng, T. Huang, Z. Liu, G. Li and L. Duan, Approaching nearly 40% external quantum efficiency in organic light emitting diodes utilizing a green thermally activated delayed fluorescence emitter with an extended linear donor–acceptor–donor structure, *Adv. Mater.*, 2021, **33**, 2103293.
34 Y. Xu, Q. Wang, X. Cai, C. Li and Y. Wang, Highly efficient electroluminescence from narrowband green circularly polarized multiple resonance thermally activated delayed fluorescence enantiomers, *Adv. Mater.*, 2021, **33**, 2100652.
35 Z. Cai, X. Wu, H. Liu, J. Guo, D. Yang, D. Ma, Z. Zhao and B. Z. Tang, Realizing record-high electroluminescence efficiency of 31.5% for red thermally activated delayed fluorescence molecules, *Angew. Chem., Int. Ed.*, 2021, **60**, 23635–23640.
36 D. Karthik, Y. H. Jung, H. Lee, S. Hwang, B. M. Seo, J. Y. Kim, C. W. Han and J. H. Kwon, Acceptor–donor–acceptor-type orange-red thermally activated delayed fluorescence materials realizing external quantum efficiency over 30% with low efficiency roll-off, *Adv. Mater.*, 2021, **33**, 2007724.
37 C. Murawski, K. Leo and M. C. Gather, Efficiency roll-off in organic light-emitting diodes, *Adv. Mater.*, 2013, **25**, 6801–6827.
38 S. Y. Byeon, D. R. Lee, K. S. Yook and J. Y. Lee, Recent progress of singlet-exciton-harvesting fluorescent organic light-emitting diodes by energy transfer processes, *Adv. Mater.*, 2019, **31**, 1803714.
39 J. H. Kim, S. H. Han and J. Y. Lee, Concentration quenching resistant donor-acceptor molecular structure for high efficiency and long lifetime thermally activated delayed fluorescent organic light-emitting diodes via suppressed non-radiative channel, *Chem. Eng. J.*, 2020, **395**, 125159.
40 J. Zhao, X. Chen, Z. Yang, Z. Chi, Z. Yang, Y. Zhang, J. Xu, Z. Chi and M. P. Aldred, Highly-efficient fully non-doped white organic light-emitting diodes consisting entirely of thermally activated delayed fluorescence emitters, *J. Mater. Chem. C*, 2018, **6**, 3226–3232.
41 R. Jakubiak, C. J. Collison, W. C. Wan and L. J. Rothberg, Aggregation quenching of luminescence in electroluminescent conjugated polymers, *J. Phys. Chem. A*, 1999, **103**, 2394–2398.
42 C. Li, R. Duan, B. Liang, G. Han, S. Wang, K. Ye, Y. Liu, Y. Yi and Y. Wang, Deep-red to near-infrared thermally activated delayed fluorescence in organic solid films and electroluminescent devices, *Angew. Chem., Int. Ed.*, 2017, **56**, 11525.
43 C. Zhou, C. Cao, D. Yang, X. Cao, H. Liu, D. Ma, C.-S. Lee and C. Yang, Highly efficient red thermally activated delayed fluorescence emitters by manipulating the molecular horizontal orientation, *Mater. Chem. Front.*, 2021, **5**, 3209–3215.
44 D. Zhang, X. Song, M. Cai, H. Kaji and L. Duan, Versatile indolocarbazole-isomer derivatives as highly emissive emitters and ideal hosts for thermally activated delayed fluorescent OLEDs with alleviated efficiency roll-off, *Adv. Mater.*, 2018, **30**, 1705406.
45 D. Sun, S. M. Suresh, D. Hall, M. Zhang, C. Si, D. B. Cordes, A. M. Z. Slawin, Y. Olivier, X. Zhang and E. Zysman-Colman, The design of an extended multiple resonance TADF emitter based on a polycyclic amine/carbonyl system, *Mater. Chem. Front.*, 2020, **4**, 2018–2022.
46 R. Furue, T. Nishimoto, I. S. Park, J. Lee and T. Yasuda, Aggregation-induced delayed fluorescence based on donor/acceptor-tethered janus carborane triads: Unique photophysical properties of nondoped OLEDs, *Angew. Chem., Int. Ed.*, 2016, **55**, 7171–7175.
47 H. Zhao, Z. Wang, X. Cai, K. Liu, Z. He, X. Liu, Y. Cao and S.-J. Su, Highly efficient thermally activated delayed fluorescence materials with reduced efficiency roll-off and low onset voltages, *Mater. Chem. Front.*, 2017, **1**, 2039–2046.
48 J. Huang, H. Nie, J. Zeng, Z. Zhuang, S. Gan, Y. Cai, J. Guo, Z. Zhao and B. Z. Tang, Highly efficient nondoped OLEDs with negligible efficiency roll-off fabricated from aggregation-induced delayed fluorescence luminogens, *Angew. Chem., Int. Ed.*, 2017, **56**, 12971–12976.
49 J. Guo, X.-L. Li, H. Nie, W. Luo, S. Gan, S. Hu, R. Hu, A. Qin, Z. Zhao, S.-J. Su and B. Z. Tang, Achieving high-performance nondoped OLEDs with extremely small efficiency roll-off by combining aggregation-induced emission and thermally activated delayed fluorescence, *Adv. Funct. Mater.*, 2017, **27**, 1606458.
50 H. Liu, J. Zeng, J. Guo, H. Nie, Z. Zhao and B. Z. Tang, High-performance non-doped OLEDs with nearly 100% exciton use and negligible efficiency roll-off, *Angew. Chem., Int. Ed.*, 2018, **57**, 9290–9294.
51 J. Guo, J. Fan, L. Lin, J. Zeng, H. Liu, C. K. Wang, Z. Zhao and B. Z. Tang, Mechanical insights into aggregation-induced delayed fluorescence materials with anti-Kasha behavior, *Adv. Sci.*, 2019, **6**, 1801629.
52 J. Zeng, J. Guo, H. Liu, J. W. Y. Lam, Z. Zhao, S. Chen and B. Z. Tang, Aggregation-induced delayed fluorescence luminogens for efficient organic light-emitting diodes, *Chem. – Asian J.*, 2019, **14**, 828–835.
53 Y. Fu, H. Liu, X. Zhu, J. Zeng, Z. Zhao and B. Z. Tang, Efficient aggregation-induced delayed fluorescent materials based on bipolar carrier transport materials for the

fabrication of high-performance nondoped OLEDs with very small efficiency roll-off, *J. Mater. Chem. C*, 2020, **8**, 9549–9557.

54 H. Liu, H. Liu, J. Fan, J. Guo, J. Zeng, F. Qiu, Z. Zhao and B. Z. Tang, An effective design strategy for robust aggregation-induced delayed fluorescence luminogens to improve efficiency stability of nondoped and doped OLEDs, *Adv. Opt. Mater.*, 2020, **8**, 2001027.

55 H. Chen, H. Liu, P. Shen, J. Zeng, R. Jiang, Y. Fu, Z. Zhao and B. Z. Tang, Efficient sky-blue bipolar delayed fluorescence luminogen for high-performance single emissive layer WOLEDs, *Adv. Opt. Mater.*, 2021, **9**, 2002019.

56 J. Chen, J. Zeng, X. Zhu, J. Guo, Z. Zhao and B. Z. Tang, Versatile aggregation-enhanced delayed fluorescence luminogens functioning as emitters and hosts for high-performance organic light-emitting diodes, *CCS Chem.*, 2021, **3**, 230–240.

57 Y.-F. Shen, M. Li, W.-L. Zhao, Y.-F. Wang, H.-Y. Lu and C.-F. Chen, Quinoline-based TADF emitters exhibiting aggregation-induced emission for efficient non-doped organic light-emitting diodes, *Mater. Chem. Front.*, 2021, **5**, 834–842.

58 H. J. Kim, H. Kang, J. E. Jeong, S. H. Park, C. W. Koh, C. W. Kim, H. Y. Woo, M. J. Cho, S. Park and D. H. Choi, Ultra-deep-blue aggregation-induced delayed fluorescence emitters: Achieving nearly 16% EQE in solution-processed nondoped and doped OLEDs with $CIE_y < 0.1$, *Adv. Funct. Mater.*, 2021, **31**, 2102588.

59 J. Luo, Z. Xie, J. W. Y. Lam, L. Cheng, H. Chen, C. Qiu, H. S. Kwok, X. Zhan, Y. Liu, D. Zhu and B. Z. Tang, Aggregation-induced emission of 1-methyl-1,2,3,4,5-pentaphenylsilole, *Chem. Commun.*, 2001, 1740–1741.

60 P. Shen, Z. Zhuang, Z. Zhao and B. Z. Tang, AIEgens based on main group heterocycles, *J. Mater. Chem. C*, 2018, **6**, 11835–11852.

61 S. Zhen, S. Wang, S. Li, W. Luo, M. Gao, L. G. Ng, C. C. Goh, A. Qin, Z. Zhao, B. Liu and B. Z. Tang, Efficient red/near-infrared fluorophores based on benzo[1,2-*b*:4,5-*b*′]dithiophene 1,1,5,5-tetraoxide for targeted photodynamic therapy and *in vivo* two-photon fluorescence bioimaging, *Adv. Funct. Mater.*, 2018, **28**, 1706945.

62 J. Yang, Y. Gao, T. Jiang, W. Liu, C. Liu, N. Lu, B. Li, J. Mei, Q. Peng and J. Hua, Substituent effects on the aggregation-induced emission and two-photon absorption properties of triphenylamine-dibenzo[a,c]phenazine adducts, *Mater. Chem. Front.*, 2017, **1**, 1396–1405.

63 H. Nie, B. Chen, J. Zeng, Y. Xiong, Z. Zhao and B. Z. Tang, Excellent n-type light emitters based on AIE-active silole derivatives for efficient simplified organic light-emitting diodes, *J. Mater. Chem. C*, 2018, **6**, 3690–3698.

64 Y. Fu, H. Liu, D. Yang, D. Ma, Z. Zhao and B. Z. Tang, Boosting external quantum efficiency to 38.6% of sky-blue delayed fluorescence molecules by optimizing horizontal dipole orientation, *Sci. Adv.*, 2021, **7**, eabj2504.

